Received: 25 April 2023 | Revised: 13 June 2023 | Accepted: 3 July 2023

DOI: 10.1002/psp4.13010

ARTICLE

Assessment of ibrutinib scheduling on leukocyte, lymph node size and blood pressure dynamics in chronic lymphocytic leukemia through pharmacokinetic-pharmacodynamic models

Eman I. K. Ibrahim | **Mats O. Karlsson** | **Lena E. Friberg**

Department of Pharmacy, Uppsala University, Uppsala, Sweden

Correspondence
Lena E. Friberg, Department of Pharmacy, Uppsala University, Box 580, Uppsala SE-75123, Sweden.
Email: lena.friberg@farmaci.uu.se

Abstract

Ibrutinib is a Bruton tyrosine kinase (Btk) inhibitor for treating chronic lymphocytic leukemia (CLL). It has also been associated with hypertension. The optimal dosing schedule for mitigating this adverse effect is currently under discussion. A quantification of relationships between systemic ibrutinib exposure and efficacy (i.e., leukocyte count and sum of the product of perpendicular diameters [SPD] of lymph nodes) and hypertension toxicity (i.e., blood pressure), and their association with overall survival is needed. Here, we present a semi-mechanistic pharmacokinetic-pharmacodynamic modeling framework to characterize such relationships and facilitate dose optimization. Data from a phase Ib/II study were used, including ibrutinib plasma concentrations to derive daily 0–24-h area under the concentration-time curve, leukocyte count, SPD, survival, and blood pressure measurements. A nonlinear mixed effects modeling approach was applied, considering ibrutinib's pharmacological action and CLL cell dynamics. The final framework included (i) an integrated model for SPD and leukocytes consisting of four CLL cell subpopulations with ibrutinib inhibiting phosphorylated Btk production, (ii) a turnover model in which ibrutinib stimulates an increase in blood pressure, and (iii) a competing risk model for dropout and death. Simulations predicted that the approved dosing schedule had a slightly higher efficacy (24-month, progression-free survival [PFS] 98%) than de-escalation schedules (24-month, average PFS ≈ 97%); the latter had, on average, ≈20% lower proportions of patients with hypertension. The developed modeling framework offers an improved understanding of the relationships among ibrutinib exposure, efficacy and toxicity biomarkers. This framework can serve as a platform to assess dosing schedules in a biologically plausible manner.

Study Highlights

WHAT IS THE CURRENT KNOWLEDGE ON THE TOPIC?

Ibrutinib is efficacious against various B-cell malignancies, but has been linked to dose-limiting hypertension on long-term therapy. Retrospective analyses have suggested that dose reductions may improve the management of adverse events without compromising the outcomes.

WHAT QUESTION DID THIS STUDY ADDRESS?

Does a stepwise reduction protocol for ibrutinib dosing reduce hypertension development without affecting the efficacy?

WHAT DOES THIS STUDY ADD TO OUR KNOWLEDGE?

A population semi-mechanistic pharmacokinetic-pharmacodynamic modeling framework was developed to characterize relationships between systemic ibrutinib exposure, leukocyte count, lymph node size, and hypertension in patients with chronic lymphocytic leukemia. The simulated cell count profiles revealed that the approved dosing schedule resulted in the highest reduction in tumor burden, whereas the de-escalation schedules had ≈20% lower proportions of simulated patients with hypertension than the approved schedule.

HOW MIGHT THIS CHANGE DRUG DISCOVERY, DEVELOPMENT, AND/OR THERAPEUTICS?

The developed semi-mechanistic framework possesses biological features that enable reliable predictions of biomarkers. Thus, this framework can be used as a time- and resource-saving tool for evaluating different dosing schedules before being tested in clinical trials.

INTRODUCTION

Ibrutinib is a first-in-class Bruton tyrosine kinase (Btk) irreversible inhibitor used to treat relapsed and refractory chronic lymphocytic leukemia (CLL) at a dose level of 420 mg day^{-1} orally.[1] Although ibrutinib shows high efficacy against different B-cell malignancies, it has been associated with cardiovascular toxicities, including hypertension.[2] Retrospective analyses have shown that dose reductions of ibrutinib to 140–280 mg day^{-1} within 3 months from treatment initiation, due to adverse events or other causes, can minimize the adverse events without having inferior outcomes on long-term therapy.[3–6]

CLL is a form of leukemia, with diverse biological and clinical characteristics.[7] The disease is characterized by abnormal B-lymphocyte accumulation in lymphoid tissues and blood.[8] Btk plays an essential role in B cell development upon phosphorylation via B cell receptor (BCR) signaling.[1] In CLL, BCR signaling is dysregulated, resulting in an increase in the proliferation and pro-survival signals.[9] Btk has an additional stimulatory effect on CXCR4 chemokine receptors supporting CLL cells' migration and adhesion to the tumor microenvironment.[10]

Inhibition of Btk suppresses the proliferation of CLL cells and causes their detachment from the supportive microenvironment. A fraction of the detached cells undergoes apoptosis. The remaining cells redistribute from tissues into the peripheral blood where ibrutinib inhibits their ability to return to tissues leading to a transient increase in blood lymphocyte count, where they die by neglect.[11] This treatment-related lymphocytosis occurs in patients to various degrees and for different durations. Previous studies have suggested that patients experiencing this phenomenon could have a longer progression-free survival (PFS).[12,13]

The cardiovascular risk associated with ibrutinib is becoming a greater concern in real-world settings where patients are old and have other comorbidities.[5,14] In a recent study by Dickerson et al.,[2] over 75% of the patients developed new or worsened hypertension that was not attenuated by either ibrutinib dose adjustments or antihypertensive usage. However, the risk factors for this hypertensive effect are not well known.

A pilot study[15] evaluated a stepwise reduction in ibrutinib dosing over three 28-day cycles from 420 mg day^{-1} in cycle 1, to 280 mg day^{-1} in cycle 2, and then to 140 mg day^{-1} in cycle 3. The pharmacokinetic (PK) and pharmacodynamic (PD) analyses suggested that the dose could be lowered without reducing of the degree of Btk inhibition. They postulated that dose reductions could potentially reduce the adverse effects developing on long-term drug usage.[15] However, these findings must be confirmed in a larger study over a longer period.

A population PK-PD modeling approach can act as a useful tool to understand exposure–response

relationships, quantify the variability in the PD responses, identify factors explaining some of the variability, and evaluate the most promising dosing schedules.[16] Thus, models considering both efficacy and safety responses while accounting for some physiopharmacological concepts are required.

In this work, a population semi-mechanistic PK-PD model was developed to characterize the relationship between systemic ibrutinib exposure, phosphorylated Btk (pBtk), leukocyte dynamics, and the longitudinal sum of the product of perpendicular diameters (SPD) of lymph node measurements. In addition, the relationships between systemic ibrutinib exposure and systolic (sBP) and diastolic (dBP) blood pressures were quantified. Thereafter, different predictors for the competing risk of dropout and death were investigated in a multistate model. The developed modeling framework was used to predict outcomes of various dosing schedules of ibrutinib in patients with CLL.

PATIENTS AND METHODS

Dataset for model building

Data were obtained from a phase Ib/II study (PCYC-1102) that included 132 patients with CLL treated once daily with ibrutinib (420 mg, $n = 94$; 840 mg, $n = 38$).[7,17] Only patients with both leukocyte count and SPD measurements were included in the analysis ($n = 120$). Further details are included in Figure S1 and the Appendices S1 and S2.

The response was evaluated according to the criteria of the International Workshop on Chronic Lymphocytic Leukemia.[18] Laboratory tests and physical examinations were performed weekly for the first month, every other week for the second month, and thereafter monthly, whereas radiologic examinations were performed at the end of weeks 8, 20, 32, 48, 60, and 96. The study was conducted in accordance with the principles of the Declaration of Helsinki and the International Conference on Harmonization Guidelines for Good Clinical Practice. All patients provided written informed consent prior to enrollment. The baseline demographic and clinical characteristics of the 120 patients are summarized in Table S1.

PK-SPD–leukocyte model

A PK/PD model was fitted to the data using a nonlinear mixed-effects modeling approach. The two-compartment population PK model developed by Marostica et al.[19] was applied to derive individual post hoc PK parameters using the available ibrutinib plasma concentrations. The daily 0–24-h area under the concentration-time curve ($AUC_{0\text{-}24}$) values were derived from integration.

Both E_{max} and sigmoidal E_{max} drug effect models were tested to characterize the relationship between the daily $AUC_{0\text{-}24}$ and fully active/pBtk. The latter was included as an unobserved variable affecting both leukocyte count and SPD dynamics. Different model structures were investigated in the light of CLL biology, its intracolonial complexity, cell trafficking, and the mechanism of action of ibrutinib, in addition to previously published studies characterizing patients with prolonged lymphocytosis when treated with ibrutinib.[12,20–22]

PK–blood pressure model

Turnover models were used to describe the time-course of ibrutinib stimulation of both sBP and dBP.[23] Linear, E_{max}, and sigmoidal E_{max} drug effect models, driven by the daily $AUC_{0\text{-}24}$ values, were evaluated. The effect of antihypertensive drugs was tested as a time-varying binary covariate, either as a step function or as a function in which the antihypertensive effect gradually evolved.

Competing risk model

Competing risk analysis of dropout and death events was performed using a multistate model (see Appendix S2: Equations S1-S3).

Covariate analysis

Baseline chromosomal abnormalities (deletion [11q], deletion [13q], and deletion [17p]), immunoglobulin heavy chain variable (IGHV) mutational status, and treatment group (i.e., being either treatment-naïve [TN] or relapsed/refractory [R/R] patients at baseline) were investigated as binary categorical covariates in all PD models. Baseline age and gender were evaluated in the blood pressure and competing risk models as earlier shown to be of clinical relevance.[24–27] Furthermore, the model-predicted baselines and the model-predicted metrics for leukocyte count, SPD, sBP, and dBP dynamics from preceding visits were explored in the competing risk model. These metrics were assessed as time-varying covariates that remained constant between two visits. Further details are included in Appendices S1 and S2.

Evaluation of the de-escalation dosing schedules

The final PK/PD models were used to generate 100 replicates of the original dataset, with the same categorical covariates and baseline age distribution, to obtain sufficient sampling of the η distribution. Two de-escalation dosing schedules were evaluated; (1) 420 mg day^{-1} for cycle 1 then 280 mg day^{-1}, as well as (2) the dosing scheduled proposed in the pilot study by Chen et al.,[15] 420 mg day^{-1} for cycle 1, 280 mg day^{-1} for cycle 2, and then 140 mg day^{-1}. Different PD variables were explored for a period of 2 years and compared to the approved dosing schedule, 420 mg day^{-1}, in patients with CLL.

Exploratory analysis of PD parameters governing leukocytosis

The simulated individual parameters from the PK-SPD-leukocyte model were compared between patients who experienced leukocytosis at 1 year and those who did not, under the 420 mg day $^{-1}$ dosing schedule. For this comparison, the Wilcoxon statistical test ($p = 0.05$) was used. Here, leukocytosis at 1 year was defined as a leukocyte count greater than or equal to 11×10^9 cells·L^{-1} and a greater than or equal to 50% increase in leukocyte count compared to baseline between the first day of month 11 and the last day of month 13.[13,28]

Model development and evaluation

All analyses were performed using R-studio (version 4.1.3). The nlmixr R package (version 2.0.6) was used for nonlinear mixed effects model development to estimate the PK-SPD-leukocyte and blood pressure models' parameters. The msm R package (version 1.6.9) was used for the competing risk analysis. The simulations were performed using the RxODE R package (version 1.1.4). Further details are included in Appendices S1 and S2.

Visual predictive checks (VPCs) were generated by simulating 500 datasets to evaluate the models' predictive performance.

RESULTS

PK-SPD–leukocyte model

The developed integrated semi-mechanistic PK-SPD-leukocyte model (Figure 1) included five ordinary differential equations (ODEs). One compartment (ODE) represented the turnover of pBtk as a relative quantity (Equation 1). Four subpopulations of CLL cells were identified, each represented by a different compartment (see Appendix S2, Equations S4-S7). $CLL_{subpop,1}$ and $CLL_{subpop,2}$ correspond to colonies of proliferating CLL cells attached to the stroma within the lymphoid tissues, with different responses to ibrutinib. These cells can be released to the surrounding microenvironment and activated into a third type ($CLL_{subpop,3}$) that can exit the lymphoid tissues and reach the peripheral blood to enter a resting state (CLL_{bld}).

A pseudo-steady state assumption was used to initialize the ODE system in the absence of ibrutinib, where the re-distribution rate constant of CLL cells from lymphoid tissues to peripheral blood (k_{dist}) was defined as follows:

$$CLL_{subpop,3,baseline} = frc2 * CLL_{tiss,baseline}$$

$$k_{dist} = \left(k_h + k_{d,bld}\right) * \frac{CLL_{bld,baseline}}{CLL_{subpop,3,baseline}}$$

where k_h represents the homing rate constant of CLL_{bld} from peripheral blood to lymphoid tissues; $k_{d,bld}$ represents the natural death rate constant of CLL_{bld}; $CLL_{tiss,baseline}$ represents the total number of proliferating CLL cells in lymphoid tissues, and frc2 represents the fraction of $CLL_{subpop,3}$ of $CLL_{tiss,baseline}$.

Upon exposure to ibrutinib, the pBtk production was inhibited using an inhibitory E_{max} model as a function of the daily $AUC_{0\text{-}24}$ values. This inhibition resulted in the following: (1) a suppression of CLL cell proliferation in lymphoid tissues, (2) apoptosis of the $CLL_{subpop,3}$ cells with an estimated half-life of 3.92 days, (3) an estimated 12.3 and 1.1-fold enhancement of the detachment rate from the stroma to the surrounding microenvironment for $CLL_{subpop,1}$ and $CLL_{subpop,2}$, respectively, compared to the normal rate (k_{dtch}), resulting in increased re-distribution of cells from lymphoid tissues to peripheral blood, and (4) a blockage of the CLL cells' ability to home back to lymphoid tissues from peripheral blood. In systemic circulation, CLL cells were estimated to die by neglect with a half-life of 90.8 days. Resistance to ibrutinib was identified for its effect on the proliferation and apoptosis of CLL cells, where the drug effect was estimated to decline exponentially with time (t) with a half-life of 761 days.

$$R_{in,pBTK} = k_{out,pBTK} * pBTK_{baseline}$$

$$EFF_{AUC0-24,pBTK} = \frac{IMAX * AUC_{0-24}}{IAUC_{50,pBTK} + AUC_{0-24}}$$

$$\frac{d(pBTK)}{dt} = R_{in,pBTK} * \left(1 - EFF_{AUC0-24,pBTK}\right) - k_{out,pBTK} * pBTK \quad (1)$$

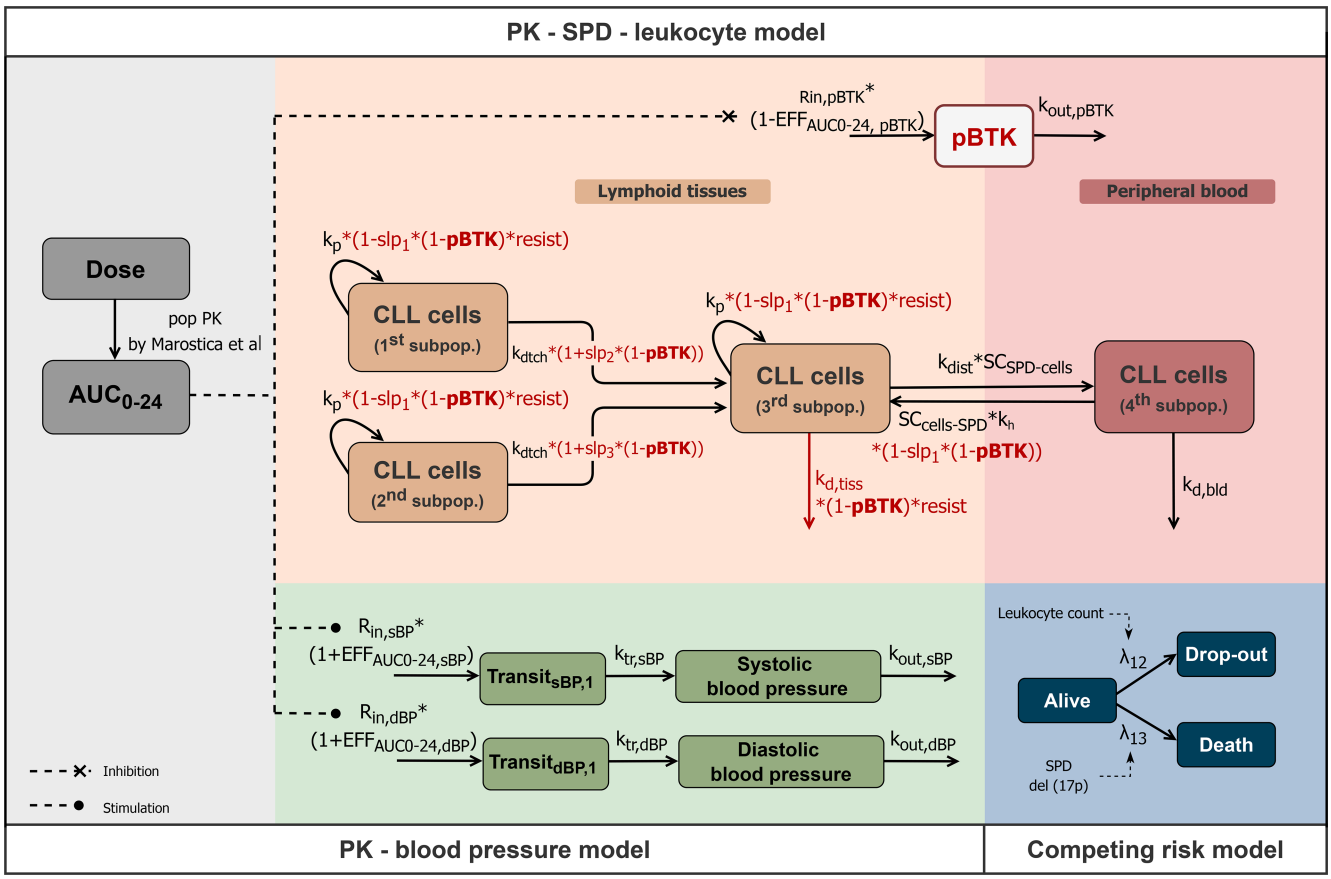

FIGURE 1 Schematic representation of the semimechanistic PK-PD modeling framework for ibrutinib in patients with CLL. Leukocyte count was calculated as the sum of the CLL cells in peripheral blood (fourth subpopulation) and the estimated normal leukocyte number in peripheral blood divided by blood volume, whereas SPD was calculated as the sum of the three subpopulations of CLL cells in lymphoid tissues and the estimated normal lymph node size. Abbreviations: $AUC_{0\text{-}24}$, 0–24-h area under the concentration-time curve; CLL, chronic lymphocytic leukemia ; dBP, diastolic blood pressure; $EFF_{AUC0\text{–}24}$, $AUC_{0\text{-}24}$ effect ; k_h, homing rate constant ; $k_{d,bld}$, natural death rate constant ; $k_{d,tiss}$, ibrutinib-induced death rate constant ; k_{dist}, re-distribution rate constant ; k_{dtch}, detachment rate constant ; k_{out}, turn-over rate constant; k_{tr}, transition rate constant ; k_p, proliferation rate constant; pBTK, phosphorylated Btk; PK, pharmacokinetic; PopPK, population pharmacokinetic ; *resist*, resistance development; R_{in}, zero-order production rate ; S_{BP}, systolic blood pressure; $SC_{cells-SPD}$ and $SC_{SPD-cells}$, scaling factors for translating from CLL cell count to SPD and vice versa, respectively ; slp_1, slope of ibrutinib-induced inhibitory effect on k_p and k_h ; slp_2 and slp_3, slopes of ibrutinib-induced stimulatory effect on k_{dtch} of first and second subpopulations of CLL cells, respectively, from stroma; SPD, sum of the product of perpendicular diameter; λ_{12}, transition rate constant from alive to drop-out state; λ_{13}, transition rate constant from alive to death state.

where $R_{in,pBTK}$ represents the production rate of pBTK; $k_{out,pBTK}$ represents the turnover rate constant of pBTK; IMAX represents the maximum inhibition of $R_{in,pBTK}$ by ibrutinib and $IAUC_{50,pBTK}$ represents the $AUC_{0\text{-}24}$ at which 50% of the maximum inhibition effect is achieved.

The effect of ibrutinib on pBtk and kinetics-related parameters were shared between both the SPD and leukocyte models producing a joint model describing CLL cell dynamics in both lymphoid tissues and peripheral blood. Particularly, SPD measurements provide information on CLL cell dynamics in lymphoid tissues, whereas leukocyte measurements provide information on their dynamics in peripheral blood. The translation between these two types of measurements was implemented using two scaling factors: (1) ($SC_{cells-SPD}$) for translating from CLL cell count to SPD, calculated as the ratio between the individual model-estimated $SPD_{baseline}$ and $CLL_{tiss,baseline}$, and (2) ($SC_{SPD-cells}$) in the opposite direction which is the reciprocal of ($SC_{cells-SPD}$).

At the end, the systemic leukocyte count was calculated as the sum of CLL_{bld} and the estimated normal leukocyte number (NRM_{bld}) in the peripheral blood divided by the blood volume. SPD was calculated as the sum of $CLL_{subpop,1}$, $CLL_{subpop,2}$ and $CLL_{subpop,3}$ in lymphoid tissues and the estimated normal lymph node size (NRM_{LN}).

In the multivariate covariate analysis, IGHV-unmutated patients were estimated to have a 2.5-fold higher $SPD_{baseline}$

than IGVH-mutated patients and TN patients were estimated to have a 1.9-fold higher NRM_{bld} compared to R/R patients.

The final model parameters and their uncertainties are presented in Table 1. The model adequately described both the observed SPD and leukocyte count data as assessed by simulation-based diagnostics (Figure 2).

PK–blood pressure model

A turnover model combined with a single transit compartment and a stimulatory effect of ibrutinib exposure on the zero-order rates for sBP and dBP response production ($R_{in,iBP}$, with index $i=s$ and d representing sBP and dBP, respectively) described the blood pressure data the best

TABLE 1 The PK–SPD–leukocyte model's parameter estimates.

Parameters	Estimate	95% CI	CV%[a]
$pBTK_{baseline}$ (%)	100 FIX	-	-
$k_{out,pBTK}$ (day^{-1})	1.35	(0.965–1.88)	282
$CLL_{bld,0}$ ($\times 10^9$ cells)	64.1	(37–112.2)	727
$CLL_{tiss,baseline}$ ($\times 10^9$ cells)	2090	(1320–3320)	55.7
$SPD_{unm,baseline}$ (cm^2)	48.9	(31.5–75.1)	132[b]
$SPD_{m,baseline}$ (cm^2)	19.5	(6.68–57.4)	132[b]
$NRM_{bld,TN}$ ($\times 10^9$ cells)	32.9	(13.2–81.9)	67.2
$NRM_{bld,RR}$ ($\times 10^9$ cells)	17.3	(12.1–24.8)	67.2
NRM_{LN} (cm^2)	2.19	(1.25–3.82)	94.9[b]
V_{Bld} (L)	5 FIX	-	-
frc1	0.471	(0.326–0.621)	162
frc2	0.208	(0.123–0.331)	177
k_p (day^{-1})[c]	0.00416	(0.00301–0.00577)	85.1
k_h (day^{-1})	0.469	(0.273–0.805)	208
$k_{d,bld}$ (day^{-1})	0.00763	(0.00319–0.0182)	92.1
IMAX	1 FIX	-	-
$IAUC_{50,pBTK}$ ($h{\cdot}ng{\cdot}mL^{-1}$)	34.1	(16.5–70.7)	297
$k_{d,tiss}$ (day^{-1})	0.177	(0.0972–0.322)	195
slp_1	1 FIX	-	-
slp_2	11.3	(7.32–17.5)	-
slp_3	0.0983	(0.0423–0.229)	-
λ_{dec} (day^{-1})	0.000911	(0.000489–0.0017)	112
Box-Cox for $CLL_{bld,baseline}$ and $SPD_{baseline}$ random effects	−0.193	(−0.398–0.0114)	-
RUV SPD (%)[d]	20	-	-
RUV leukocyte count (%)[d]	22	-	-

Abbreviations: CI, confidence interval; $CLL_{bld,baseline}$, baseline CLL cells in peripheral blood; $CLL_{tiss,baseline}$, baseline total number of proliferating CLL cells in lymphoid tissues; frc1, fraction of the CLL cells 2nd subpopulation of total CLL cells attached to the stroma; frc2, fraction of the CLL cells 3rd subpopulation of $CLL_{tiss,baseline}$; CV%, coefficient of variation percentage; $IAUC_{50,pBTK}$, $AUC_{0\text{-}24}$ at which 50% of maximum inhibition effect is achieved; IMAX, maximum inhibition of pBtk production rate by ibrutinib; $k_{d,bld}$, natural death rate constant of CLL cells in peripheral blood; $k_{d,tiss}$, ibrutinib-induced death rate constant of CLL cells in lymphoid tissues; k_h, homing rate constant of CLL cells from peripheral blood to lymphoid tissues; $k_{out,pBTK}$, turn-over rate constant of pBtk; k_p, proliferation rate constant of CLL cells; $NRM_{bld,TN}$ and $NRM_{bld,RR}$; normal leukocyte number in treatment-naïve and relapsed refractory patients, respectively; NRM_{LN}, normal lymph nodes' size; $pBTK_{baseline}$, baseline phosphorylated Btk value; PK, pharmacokinetic; SPD, sum of the product of perpendicular diameters; $SPD_{unm,baseline}$ and $SPD_{m,baseline}$; baseline SPD in IGVH unmutated- and mutated-patients, respectively; slp_1, slope of ibrutinib-induced inhibitory effect on k_p and k_h; slp_2 and slp_3, slopes of ibrutinib-induced stimulatory effect on the detachment rates (k_{dtch}) of first and second subpopulations of CLL cells, respectively, from stroma; V_{bld}, blood volume; λ_{dec}, exponential decay constant of ibrutinib effect over time.

[a]Co-efficient of variation (CV) $= \sqrt{\exp(\omega^2) - 1}$.

[b]The 63% estimated correlation between ω^2 for $SPD_{baseline}$ and NRM_{LN}.

[c]k_{dtch} was assumed to be equal to k_p.

[d]Additive residual unexplained variability (RUV) model was implemented on log transformed data.

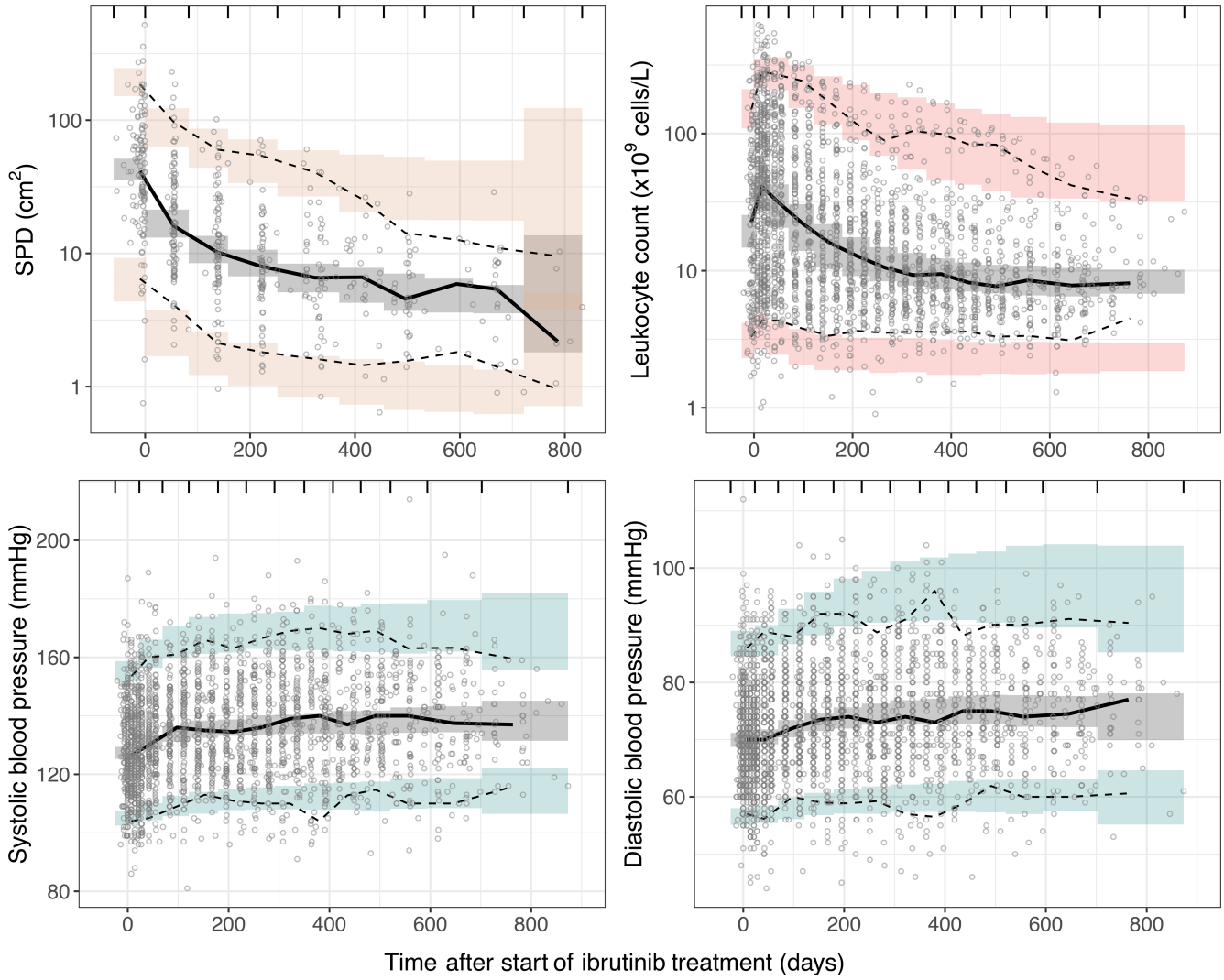

FIGURE 2 Visual predictive checks of the PK-SPD-leukocyte model (upper panel), taking competing risk of dropout and death into account, and the PK-blood pressure models (lower panel). Gray points are the observations. Solid black lines are the median of the observations. Dashed black lines are the 5th and 95th percentiles of the observations. The CIs are constructed based on 500 datasets simulated from the final models. Gray shaded areas are the 90% CI of the predicted median. Orange, pink, and green shaded areas are the 90% CIs of the 5th and 95th percentiles for SPD, leukocyte count and blood pressure, respectively. CI, confidence interval; PK, pharmacokinetic; SPD, sum of the product of perpendicular diameters.

(Equations 2 and 3). The stimulatory effect was characterized using an E_{max} model as a function of the daily $AUC_{0\text{-}24}$. The turnover rate constant ($k_{out,iBP}$) was assumed to be equal to the transition rate constant ($k_{tr,iBP} = \frac{(n+1)}{MTT_{iBP}}$, where MTT_{iBP} is the mean transit time and n is the number of transit compartments).

$$R_{in,iBP} = k_{out,iBP} * iBP_{baseline}$$

$$EFF_{AUC0-24,iBP} = \frac{E_{max,iBP} * AUC_{0-24}}{AUC_{50,iBP} + AUC_{0-24}}$$

$$\frac{d(transit_{iBP,1})}{dt} = R_{in,iBP} * (1 + EFF_{AUC0-24,iBP}) - k_{tr,iBP} * transit_{iBP,1} \quad (2)$$

$$\frac{d(iBP)}{dt} = k_{tr,iBP} * transit_{iBP,1} - k_{out,iBP} * iBP \quad (3)$$

where $E_{max,iBP}$ represents the maximum ibrutinib stimulatory effect, and $AUC_{50,iBP}$ represents the $AUC_{0\text{-}24}$ at which 50% of the maximum stimulation effect is achieved.

According to the multivariate covariate analysis, patients with a higher baseline age had lower MTT_{sBP} and dBP_0. The final model parameters and their uncertainties are presented in Table 2. The VPCs (Figure 2) show that both the sBP and dBP models well-predicted the overall increase in BP and the variability on the long-term use of ibrutinib.

TABLE 2 The PK–blood pressure and competing risk models' parameter estimates.

Parameters	Estimate	95% CI	CV%[a]
Blood pressure model			
$sBP_{baseline}$ (mmHg)	126	(124–129)	8.28
$dBP_{baseline}$ (mmHg)	69.7	(68.5–70.9)	9.02
MTT_{sBP} (days)	79.9	(67.3–94.9)	123
MTT_{dBP} (days)	161	(106–244)	-
$E_{max,sBP}$	0.113	(0.092–0.139)	52
$E_{max,dBP}$	0.0694	(0.0482–0.1)	107
$AUC_{50,sBP}$ ($h \cdot ng \cdot mL^{-1}$)	91.7	(42.1–200)	-
$AUC_{50,dBP}$ ($h \cdot ng \cdot mL^{-1}$)	63.1	(9.75–408)	-
Coefficient of baseline age effect on $dBP_{baseline}$[b]	−0.204	(−0.298 to −0.111)	-
Coefficient of baseline age effect on MTT_{sBP}[c]	−5.04	(−6.07 to −4)	-
RUV sBP (%)[d]	8.4	-	-
RUV dBP (%)[d]	8.9	-	-
Competing risk model			
λ_{12} ($month^{-1}$)	0.00908	(0.0053–0.0155)	-
λ_{13} ($month^{-1}$)	0.00275	(0.00102–0.00743)	-
Coefficient of past model-predicted leukocyte count on λ_{12}[e]	−0.89	(−1.47 to −0.304)	-
Coefficient of past model-predicted SPD on λ_{13}[f]	0.563	(0.077–1.05)	-
Coefficient of deletion (17p) on λ_{12}[f]	1.42	(0.153–2.7)	-

Abbreviations: $AUC_{50,sBP}$ and $AUC_{50,dBP}$, $AUC_{0\text{-}24}$ at which 50% of maximum stimulation effect is achieved; CI, confidence interval; CV%, coefficient of variation percentage; $E_{max,sBP}$ and $E_{max,dBP}$, maximum ibrutinib stimulatory effect; MTT_{sBP} and MTT_{dBP}, mean transit time; PK, pharmacokinetic; $sBP_{baseline}$ and $dBP_{baseline}$, baseline sBP and dBP, respectively; λ_{12}, transition rate constant from alive to drop-out state; λ_{13}, transition rate constant from alive to death state.

[a]Co-efficient of variation (CV) $= \sqrt{\exp(\omega^2) - 1}$.

[b]$dBP_{baseline} = e^{\left(LN(69.7) - 0.204 * LN\left(\frac{Age}{63}\right)\right)}$.

[c]$MTT_{sBP} = e^{\left(LN(79.9) - 5.04 * LN\left(\frac{Age}{63}\right)\right)}$.

[d]Additive residual unexplained variability (RUV) model was implemented on log transformed data.

[e]$\lambda_{12} = 0.00908 * e^{\left(-0.89 * LN\left(\frac{Leukocyte}{12}\right)\right)}$.

[f]$\lambda_{13} = 0.00275 * e^{\left(0.563 * LN\left(\frac{SPD}{14}\right) + 1.42 * (del(17p))\right)}$.

Competing risk model

A multistate model was successfully developed to characterize the marginal probability of a dropout event in the presence of a competing death event, and vice versa. The transition rate to the dropout state was increasing with the decline in the past model-predicted leukocyte count (hazard ratio [HR] = 4.92 for every 10-unit decrease in the leukocyte count). Moreover, the past model-predicted SPD was predictive of the transition rate to the death state (HR = 1.35 for every 10-unit increase in SPD). Patients carrying deletion (17p) chromosomal abnormality had a statistically significant higher probability of death than patients without (HR = 4.16). The final model parameters together and their uncertainties are presented in Table 2. Kaplan–Meier VPCs for dropout and overall survival (OS; Figure 3) illustrate the adequate predictive properties of the model, with the exception of the apparent mis-fit near the study end, which are due to the low number of patients observed in the timeframe of 25–30 months.

Evaluation of the de-escalation dosing schedules

Simulated SPD and leukocyte count profiles (Figure S2) suggested that there are minor differences between the evaluated dosing schedules at the 10th and 50th percentiles

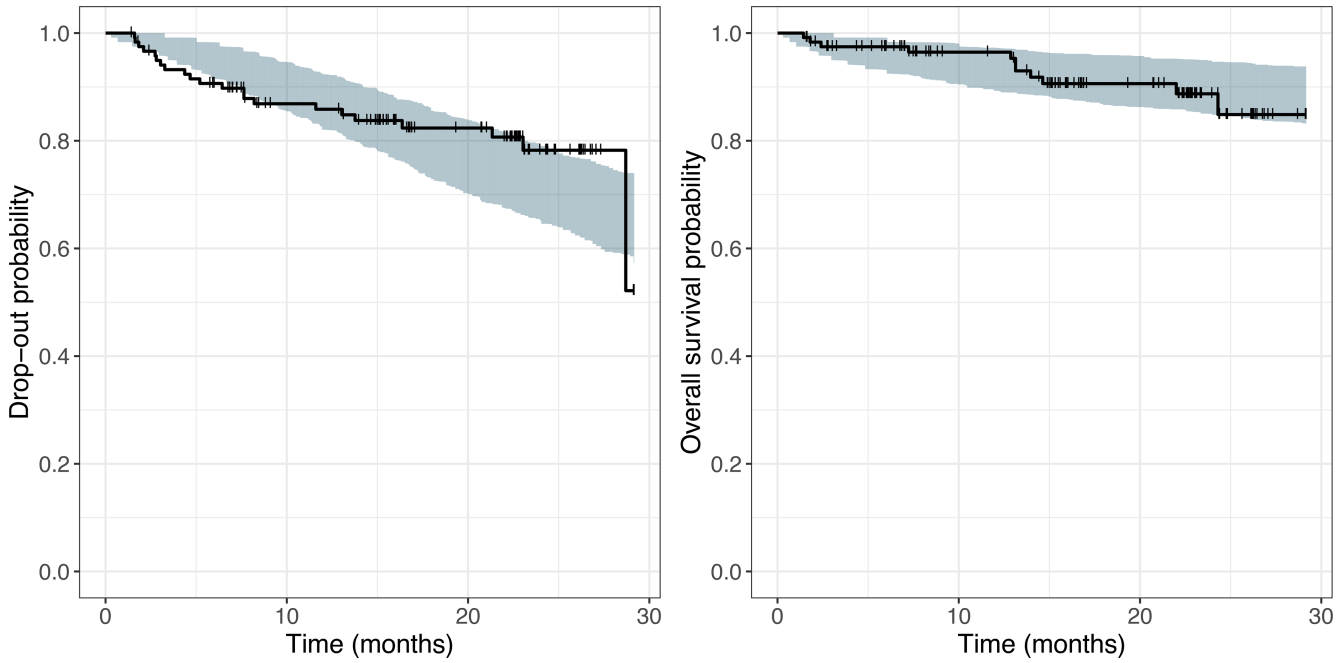

FIGURE 3 Kaplan–Meier visual predictive checks for the dropout probability (left panel) and overall survival (right panel) based on the competing risk model. The observed Kaplan–Meier curve (black line) is compared to the 90% confidence interval (shaded blue) derived from 500 model simulations.

of the simulation interval. However, at the 90th percentile in the model-predicted SPD time profiles, the approved dosing schedule had the highest efficacy, whereas the de-escalation schedule 2 had the lowest efficacy. This finding was more pronounced in the simulated total tumor burden profiles (Figure 4). The simulated time-courses of the four subpopulations are also shown in Figure S3. Furthermore, the approved dosing schedule had 92.7% (80% confidence interval [CI], 56.8%–99%) Btk occupancy, calculated as (1-pBtk)*100, on the last day of cycle 3, whereas the de-escalation schedules 1 and 2 had 89.4% (80% CI, 46.8%–98.7%) and 80.8% (80% CI, 30.4%–97.4%) Btk occupancy, respectively (Figure S4).

The PFS analyses were performed on the simulated data, with progression defined as an increase of greater than or equal to 50% from nadir in SPD with or without leukocytosis. IGVH-mutated patients on the de-escalation dosing schedules studied had a slightly higher PFS compared to IGVH-unmutated patients (Figure S5). Patients with leukocyte count greater than or equal to 11×10^9 cells·L^{-1} at week 4 had better PFS (24-month, PFS 98.4%, 98.1%, and 97.7% for the approved, de-escalation schedules 1 and 2, respectively) compared to patients with lower leukocyte count (24-month, PFS 95.7%, 95.3%, and 93.7% for the approved, de-escalation schedules 1 and 2, respectively); however, the observed differences were less at week 8 (Figure S6).

The de-escalation schedule proposed by Chen et al. pilot study had a beneficial effect on blood pressure

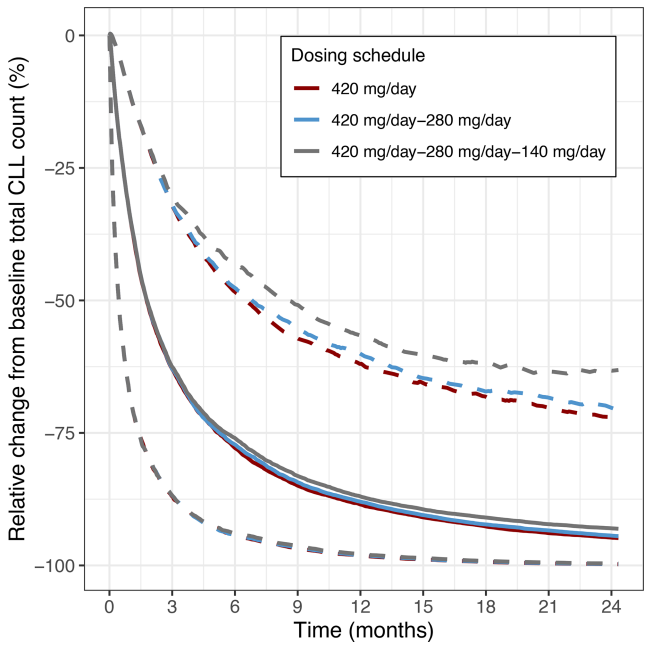

FIGURE 4 Simulations from the PK-SPD-leukocyte model illustrated as a summary of the relative change of the individual predictions of total CLL count from their baselines over time. Solid lines are the median and dashed lines are the 10th and 90th percentiles of the simulation intervals. Colors represent the different investigated dosing schedules; (1) 420 mg day^{-1} (red), (2) 420 mg day^{-1} in cycle 1 then 280 mg day^{-1} (blue), and (3) 420 mg day^{-1} in cycle 1, 280 mg day^{-1} in cycle 2 then 140 mg day^{-1} (gray). One cycle is 28-days. CLL, chronic lymphocytic leukemia; PK, pharmacokinetic; SPD, sum of the product of perpendicular diameters.

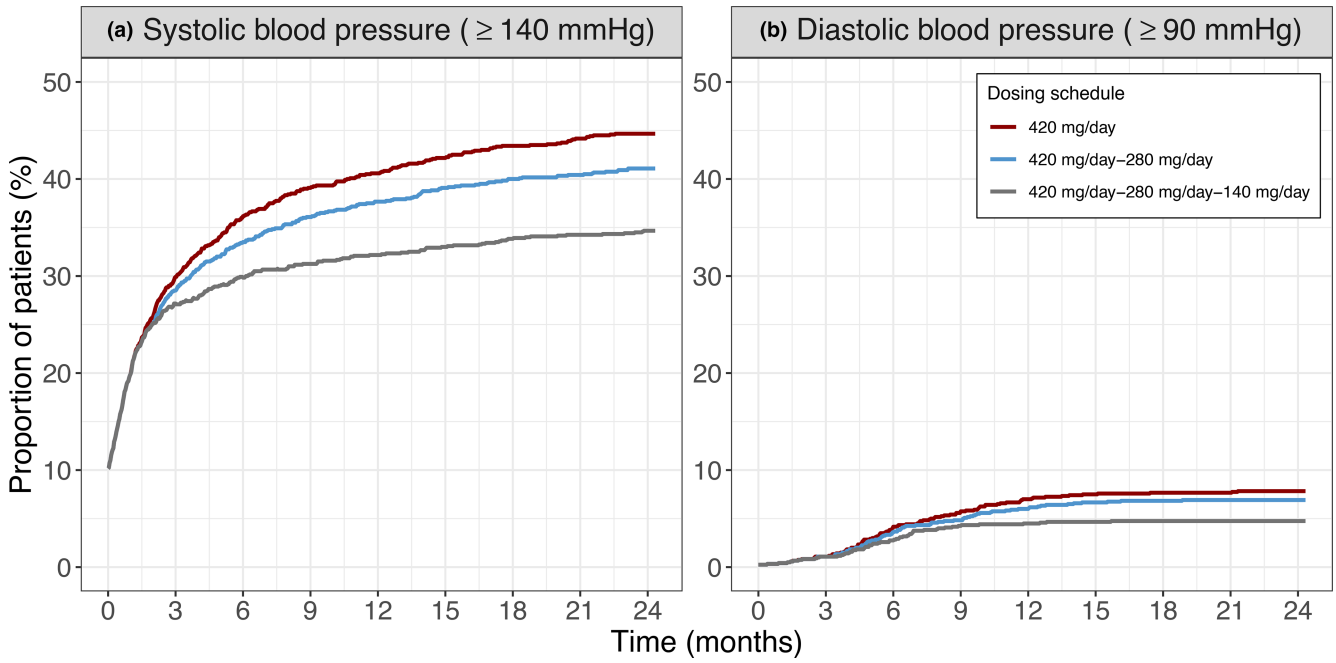

FIGURE 5 Predictions from the PK-blood pressure models of the proportions of patients experiencing; (a) greater than or equal to 140 mmHg systolic blood pressure, and (b) greater than or equal to 90 mmHg diastolic blood pressure. Colors represent the different investigated dosing schedules; (1) 420 mg day^{-1} (red), (2) 420 mg day^{-1} in cycle 1 then 280 mg day^{-1} (blue), and (3) 420 mg day^{-1} in cycle 1, 280 mg day^{-1} in cycle 2 then 140 mg day^{-1} (gray). One cycle is 28-days. PK, pharmacokinetic.

profiles (Figure S2), particularly at the 90th percentile of the simulation interval, as it had the lowest relative change from baseline during the treatment period. At baseline, 10.2% and 0.25% of the patients had sBP greater than or equal to 140 mmHg and dBP greater than or equal to 90 mmHg[2] in all the investigated dosing schedules, respectively, whereas at 2 years, 44.7%, 41.1%, and 34.7% of the patients had sBP greater than or equal to 140 mmHg and 7.83%, 6.92%, and 4.75% of the patients had dBP greater than or equal to 90 mmHg under the approved, de-escalation dosing schedules 1 and 2, respectively (Figure 5).

Exploratory analysis of PD parameters governing leukocytosis

The simulated individual estimates of $k_{d,bld}$, $k_{d,tiss}$, λ_{dec}, $IAUC_{50,pBTK}$, $CLL_{tiss,0}$, and frc2 were statistically different between patients who did and did not experience leukocytosis at 1 year (Figure S7). The median values of the simulated $k_{d,bld}$, $k_{d,tiss}$, $IAUC_{50,pBTK}$, and frc2 estimates were 1.69-, 3.66-, 2.11-, and 2.29-fold higher, respectively, in patients experiencing no leukocytosis in comparison to patients experiencing it at 1 year, whereas the median values of λ_{dec} and $CLL_{tiss,0}$ in patients without leukocytosis were 0.686 and 0.877, respectively, times those values in patients with it.

DISCUSSION

The developed population PK-PD models successfully quantified the relationships among ibrutinib exposure, represented by daily $AUC_{0\text{-}24}$, and leukocyte count along with SPD, sBP, and dBP dynamics, while considering the mechanism of action of ibrutinib. AUC_{0-24} was chosen as the PK driver because it has previously been proposed as a surrogate of plasma exposure and a metric for therapeutic drug monitoring of ibrutinib owing to its short half-life (4–13 h).[29,30] The semi-mechanistic PK-SPD-leukocyte model identified four subpopulations of CLL cells that were linked as a continuum reflecting the complexity of CLL biology and dynamics. Our model was developed to mimic the CLL cell's life cycle as proposed by Calissano et al.[22] In their work, CLL cells are assumed to be attached to the stroma through CXCR4-CXCL12 interactions (i.e., first and second subpopulations in our model). Upon BCR signaling stimulation, CLL cells begin to proliferate and detach from the stroma. Thereafter, CLL cells, that have recently undergone mitosis (i.e., third subpopulation in our model), exit lymphoid tissues into the peripheral blood. Over time, resting CLL cells in peripheral blood will re-express CXCR4 enabling them to return to the lymphoid tissues. Furthermore, a competing risk model characterized adequately the competing dropout and death events.

Given the importance of Btk in CLL cell development and the previously reported wide variability in its de

novo synthesis rate between patients (range 3.6%–31.4% day^{-1}),[31] the unobserved time-course of pBtk constituted an influential component in the developed framework. Its turnover rate constant was estimated (135% day^{-1}, range 13.8%–417% day^{-1}) to describe the time-delay until the full Btk inactivation by ibrutinib is achieved, as well as the return of fully active Btk to its normal level after the treatment discontinuation, requiring Btk de novo synthesis. However, the model overestimated the turnover rate. This could be because it used the daily $AUC_{0\text{-}24}$ to assess the exposure-response relationship, but if the full plasma concentration-time profile was used instead, we might have seen a slower turnover rate.[30] Moreover, for a dose of 420 mg day^{-1}, the median simulated Btk occupancy was 92.7% (80% CI, 56.8%–99%) at steady-state, which is close to the previously reported median target occupancy for ibrutinib (range 96%–99%) for dose levels 420 and 840 mg day^{-1}.[7,32]

Here, ibrutinib was assumed to be able to completely inhibit both CLL cell proliferation and homing given the previously reported effective suppression of these two processes by ibrutinib.[33] In addition, we estimated an average proliferation rate constant of 0.416% day^{-1}, a death rate constant in peripheral blood of 0.763% day^{-1}, and in tissues of 17.7% day^{-1}, all of which were in a close agreement with prior knowledge of CLL progression and treatment response. Burger et al.[11] concluded an average proliferation rate constant of 0.39% day^{-1} (range 0.17%–1.04%) decreasing to 0.05% day^{-1} (range 0%–0.36%) with ibrutinib and an average death rate constant of 1.5% day^{-1} (range 0%–3%) in peripheral blood. Furthermore, they determined an average rate constant of $28.88\% \pm 11.33\%$ day^{-1} and $12.06\% \pm 9.42\%$ day^{-1} for CLL cell death in tissues of IGHV-unmutated and IGHV-mutated patients with CLL, respectively.

Our analysis showed that the drug effect decreased exponentially with a half-life of 761 days. Notably, only ibrutinib-induced CLL cell death in tissues and inhibition of its proliferation were significantly influenced by such resistance. A study by Ahn et al.[34] reported that histologic transformation was the driver for the early development of resistance to ibrutinib whereas resistance developing later in the treatment course was associated with Btk and/or PLCG2 mutations.

Identifying two subpopulations of CLL cells that detach from the stroma, the second of which detaches at a rate 115 times slower than the first one, explained the observed bi-exponential decay in SPD during the treatment period. This second subpopulation in combination with the slow estimated individual CLL cell death rate in tissues and peripheral blood characterized the long-term stabilization of leukocyte count observed in some patients, as illustrated in the exploratory analysis of simulated PD parameters. The way the model was structured to describe this stabilization is consistent with previous studies revealing that CLL cells encountered during this stabilization phase are quiescent rather than carrying resistance mutations.[12,33,35] These patients may benefit the most from the combination of ibrutinib and venetoclax, which works by reactivating the apoptosis of resting CLL cells.[36,37]

A turnover model, combined with a single transit compartment, could quantify the nonlinear exposure-blood pressure relationship, along with the slow onset of this adverse event as demonstrated previously.[2,38] The higher the E_{max} for sBP with a 2.01-fold faster onset than that for dBP is consistent with previous conclusions.[2,38] Although the exact mechanism underlying this adverse event is unknown, several hypotheses have been proposed. These include endothelial dysfunction, decreased nitric oxide production, and inhibition of the PI3K/Akt pathway by ibrutinib causing vascular tissue fibrosis and cellular remodeling.[2]

The baseline dBP was inversely correlated with age, as previously described,[24] and older patients had lower MTT_{sBP} values. Patients who had deletion (17p) chromosomal abnormality had 313% higher risk of dying than those patients who did not, which agrees with previous findings that these patients were in the high-risk CLL subgroup (10-year OS, 29%).[13,39–41] Patients with last observed model-predicted leukocyte counts lower than the normal count, potentially because of neutropenia,[7] were more likely to drop out. In addition, the last observed model-predicted tumor size was predictive of death events (i.e., the larger the SPD, the higher the hazard of death). This finding is in line with the correlation between the number of involved lymph node sites and survival in patients with untreated CLL.[42]

The simulation results illustrated that the approved dosing schedule had the highest efficacy in terms of the ibrutinib-induced reduction of the total CLL cell count. When compared to the de-escalation schedule proposed by Chen et al.,[15] however, it showed a higher probability of developing hypertension, with 29% and 65% higher risks of experiencing sBP greater than or equal to 140 mmHg and dBP greater than or equal to 90 mmHg at 2-years, respectively. This finding is attributed to the fact that the $AUC_{50,sBP}$ and $AUC_{50,dBP}$ are approximately three and two times higher than $IAUC_{50,pBTK}$, respectively, as well as the slow turnover rates of sBP and dBP. Further, patients having more than 80% simulated target occupancy with the low dose (140 mg day^{-1}) achieved the same level of efficacy in terms of SPD reduction as those with higher dose levels. In addition, IGHV-mutated patients had, on average, 98.6% PFS at 2-years across all evaluated dosing schedules, which could be attributed to lower SPD_0 according to the covariate analysis results. This finding is

further supported in Figure S4 where PFS is stratified on baseline SPD with a cutoff of 50 cm^2.[43]

There are a number of previously published models quantifying CLL cell dynamics in patients with CLL under ibrutinib treatment. The first model was proposed by Wodarz et al.,[33] however, it did not consider the ibrutinib exposure level and its variability between patients. Further, Gallais et al.[44] developed a population PK-PD model of circulating lymphocyte dynamics but their model lacked a comprehensive description of the different ibrutinib's effects. Our model is the first to integrate the longitudinal SPD and leukocyte count measurements simultaneously while considering the different effects of ibrutinib on CLL cell dynamics in lymphoid tissues and peripheral blood.

One of the limitations of the presented work is that the model considered only the lymph nodes for deriving information on the CLL tissue burden and dynamics. This may not reflect the pathophysiological reality that other lymphoid tissues are involved in CLL such as spleen and bone marrow.[45] The characterization of the CLL dynamics in absence of treatment was simplified due to the limited pretreatment and off-treatment data. Despite these limitations, the graphical-based diagnostics showed that the model can adequately predict the observed clinical data at both individual (data not shown) and population levels. The model simplified the ibrutinib CLL resistance evolution due to the short study length compared to the slow resistance development,[34] that could result in an increased uncertainty of model predictions for extrapolation beyond 2 years.

To conclude, our modeling analysis succeeded in integrating two types of efficacy measurements, SPD and leukocyte count, in a joint model for characterizing CLL cell dynamics and the pharmacological action of ibrutinib. Furthermore, a relationship between ibrutinib exposure and blood pressure was established. We present a novel population semi-mechanistic PK-PD modeling framework that offers an improved understanding of the relationships between ibrutinib exposure and different efficacy and adverse drug reaction biomarkers, in addition to OS in patients with CLL. The mechanistic assumptions behind the developed framework allow it to predict different dimensions related to ibrutinib-induced effects simultaneously.[46] Thus, this framework can serve as a platform for evaluating alternative dosing schedules, as demonstrated in our simulations. Besides, it can be used as a model-informed precision dosing tool to assess dose-individualization approaches to identify safe and efficacious treatment schedules.

AUTHOR CONTRIBUTIONS

E.I.K.I., M.O.K., and L.E.F. wrote manuscript and designed research. E.I.K.I. performed research and analyzed data.

ACKNOWLEDGMENTS

This study, carried out under YODA Project 2020-4386, used data obtained from the Yale University Open Data Access Project, which has an agreement with Janssen Research & Development, L.L.C. The interpretation and reporting of research using this data are solely the responsibility of the authors and does not necessarily represent the official views of the Yale University Open Data Access Project or Janssen Research & Development, L.L.C.

FUNDING INFORMATION

This work was supported by the Swedish Cancer Society (Funding Number 20: 1226 PjF and CAN 2017/626).

CONFLICT OF INTEREST STATEMENT

The authors declared no competing interests for this work.

DISCLAIMER

As Deputy Editor-in-Chief of CPT: Pharmacometrics & Systems Pharmacology, Lena Friberg was not involved in the review or decision process for this paper.

ORCID

Eman I. K. Ibrahim https://orcid.org/0000-0002-9282-9136
Mats O. Karlsson https://orcid.org/0000-0003-1258-8297
Lena E. Friberg https://orcid.org/0000-0002-2979-679X

REFERENCES

1. Vela CM, McBride A, Jaglowski SM, Andritsos LA. Ibrutinib for treatment of chronic lymphocytic leukemia. *Am J Health Syst Pharm*. 2016;73(6):367-375. doi:10.2146/ajhp140760
2. Dickerson T, Wiczer T, Waller A, et al. Hypertension and incident cardiovascular events following ibrutinib initiation. *Blood*. 2019;134(22):1919-1928. doi:10.1182/blood.2019000840
3. Cervantes-Gomez F, Kumar Patel V, Bose P, Keating MJ, Gandhi V. Decrease in total protein level of Bruton's tyrosine kinase during ibrutinib therapy in chronic lymphocytic leukemia lymphocytes. *Leukemia*. 2016;30(8):1803-1804. doi:10.1038/leu.2016.129
4. Akhtar OS, Attwood K, Lund I, Hare R, Hernandez-Ilizaliturri FJ, Torka P. Dose reductions in ibrutinib therapy are not associated with inferior outcomes in patients with chronic lymphocytic leukemia (CLL). *Leuk Lymphoma*. 2019;60(7):1650-1655. doi:10.1080/10428194.2018.1554862
5. Hou JZ, Ryan K, Du S, et al. Real-world ibrutinib dose reductions, holds and discontinuations in chronic lymphocytic leukemia. *Future Oncol*. 2021;17(35):4959-4969. doi:10.2217/fon-2021-0964
6. Mato AR, Timlin C, Ujjani C, et al. Comparable outcomes in chronic lymphocytic leukaemia (CLL) patients treated with reduced-dose ibrutinib: results from a multi-Centre study. *Br J Haematol*. 2018;181(2):259-261. doi:10.1111/bjh.14540
7. Byrd JC, Furman RR, Coutre SE, et al. Targeting BTK with Ibrutinib in relapsed chronic lymphocytic leukemia. *N Engl J Med*. 2013;369(1):32-42. doi:10.1056/NEJMoa1215637

8. Hallek M, Cheson BD, Catovsky D, et al. iwCLL guidelines for diagnosis, indications for treatment, response assessment, and supportive management of CLL. *Blood*. 2018;131(25):2745-2760. doi:10.1182/blood-2017-09-806398
9. Woyach JA, Johnson AJ, Byrd JC. The B-cell receptor signaling pathway as a therapeutic target in CLL. *Blood*. 2012;120(6):1175-1184. doi:10.1182/blood-2012-02-362624
10. Chen SS, Chang BY, Chang S, et al. BTK inhibition results in impaired CXCR4 chemokine receptor surface expression, signaling and function in chronic lymphocytic leukemia. *Leukemia*. 2016;30(4):833-843. doi:10.1038/leu.2015.316
11. Burger JA, Li KW, Keating MJ, et al. Leukemia cell proliferation and death in chronic lymphocytic leukemia patients on therapy with the BTK inhibitor ibrutinib. *JCI Insight*. 2017;2(2):e89904. doi:10.1172/jci.insight.89904
12. Woyach JA, Smucker K, Smith LL, et al. Prolonged lymphocytosis during ibrutinib therapy is associated with distinct molecular characteristics and does not indicate a suboptimal response to therapy. *Blood*. 2014;123(12):1810-1817. doi:10.1182/blood-2013-09-527853
13. Byrd JC, Furman RR, Coutre SE, et al. Ibrutinib treatment for first-line and relapsed/refractory chronic lymphocytic leukemia: final analysis of the pivotal phase Ib/II PCYC-1102 study. *Clin Cancer Res*. 2020;26(15):3918-3927. doi:10.1158/1078-0432.CCR-19-2856
14. Abdel-Qadir H, Sabrie N, Leong D, et al. Cardiovascular risk associated with Ibrutinib use in chronic lymphocytic leukemia: a population-based cohort study. *J Clin Oncol*. 2021;39(31):3453-3462. doi:10.1200/JCO.21.00693
15. Chen LS, Bose P, Cruz ND, et al. A pilot study of lower doses of ibrutinib in patients with chronic lymphocytic leukemia. *Blood*. 2018;132(21):2249-2259. doi:10.1182/blood-2018-06-860593
16. Standing JF. Understanding and applying pharmacometric modelling and simulation in clinical practice and research. *Br J Clin Pharmacol*. 2017;83(2):247-254. doi:10.1111/bcp.13119
17. Byrd JC, Furman RR, Coutre SE, et al. Three-year follow-up of treatment-naïve and previously treated patients with CLL and SLL receiving single-agent ibrutinib. *Blood*. 2015;125(16):2497-2506. doi:10.1182/blood-2014-10-606038
18. Hallek M, Cheson BD, Catovsky D, et al. Guidelines for the diagnosis and treatment of chronic lymphocytic leukemia: a report from the international workshop on chronic lymphocytic leukemia updating the National Cancer Institute-working group 1996 guidelines. *Blood*. 2008;111(12):5446-5456. doi:10.1182/blood-2007-06-093906
19. Marostica E, Sukbuntherng J, Loury D, et al. Population pharmacokinetic model of ibrutinib, a Bruton tyrosine kinase inhibitor, in patients with B cell malignancies. *Cancer Chemother Pharmacol*. 2015;75(1):111-121. doi:10.1007/s00280-014-2617-3
20. Chen SS, Ham S, Ravichandran P, et al. In vivo evidence of in situ cell death preferentially occurring in CLL patients with minimal lymphocytosis by the diminished BCL2 and loss of T cell support after Ibrutinib treatment. *Blood*. 2016;128(22):5586. doi:10.1182/blood.V128.22.5586.5586
21. Burger JA, Montserrat E. Coming full circle: 70 years of chronic lymphocytic leukemia cell redistribution, from glucocorticoids to inhibitors of B-cell receptor signaling. *Blood*. 2013;121(9):1501-1509. doi:10.1182/blood-2012-08-452607
22. Calissano C, Damle RN, Marsilio S, et al. Intraclonal complexity in chronic lymphocytic leukemia: fractions enriched in recently born/divided and older/quiescent cells. *Mol Med*. 2011;17(11–12):1374-1382. doi:10.2119/molmed.2011.00360
23. Hansson E, Ma G, Amantea M, et al. PKPD modeling of predictors for adverse effects and overall survival in Sunitinib-treated patients with GIST. *CPT Pharmacomet Syst Pharmacol*. 2013;2(12):85. doi:10.1038/psp.2013.62
24. Pinto E. Blood pressure and ageing. *Postgrad Med J*. 2007;83(976):109-114. doi:10.1136/pgmj.2006.048371
25. Shanafelt TD, Rabe KG, Kay NE, et al. Age at diagnosis and the utility of prognostic testing in patients with chronic lymphocytic leukemia (CLL). *Cancer*. 2010;116(20):4777-4787. doi:10.1002/cncr.25292
26. Reckelhoff JF. Gender differences in the regulation of blood pressure. *Hypertension*. 2001;37(5):1199-1208. doi:10.1161/01.HYP.37.5.1199
27. Catovsky D, Wade R, Else M. The clinical significance of patients' sex in chronic lymphocytic leukemia. *Haematologica*. 2014;99(6):1088-1094. doi:10.3324/haematol.2013.101378
28. Barrientos JC, Burger JA, Byrd JC, et al. Characterizing the kinetics of lymphocytosis in patients with chronic lymphocytic leukemia treated with single-agent ibrutinib. *Leuk Lymphoma*. 2019;60(4):1000-1005. doi:10.1080/10428194.2018.1512710
29. Verheijen RB, Yu H, Schellens JHM, Beijnen JH, Steeghs N, Huitema ADR. Practical recommendations for therapeutic drug monitoring of kinase inhibitors in oncology. *Clin Pharmacol Ther*. 2017;102(5):765-776. doi:10.1002/cpt.787
30. Le Louedec F, Gallais F, Thomas F, et al. Limited sampling strategy for determination of Ibrutinib plasma exposure: joint analyses with metabolite data. *Pharmaceuticals*. 2021;14(2):162. doi:10.3390/ph14020162
31. Alsadhan A, Cheung J, Gulrajani M, et al. Pharmacodynamic analysis of BTK inhibition in patients with chronic lymphocytic leukemia treated with acalabrutinib. *Clin Cancer Res off J Am Assoc Cancer Res*. 2020;26(12):2800-2809. doi:10.1158/1078-0432.CCR-19-3505
32. Advani RH, Buggy JJ, Sharman JP, et al. Bruton tyrosine kinase inhibitor Ibrutinib (PCI-32765) has significant activity in patients with relapsed/refractory B-cell malignancies. *J Clin Oncol*. 2013;31(1):88-94. doi:10.1200/JCO.2012.42.7906
33. Wodarz D, Garg N, Komarova NL, et al. Kinetics of CLL cells in tissues and blood during therapy with the BTK inhibitor ibrutinib. *Blood*. 2014;123(26):4132-4135. doi:10.1182/blood-2014-02-554220
34. Ahn IE, Underbayev C, Albitar A, et al. Clonal evolution leading to ibrutinib resistance in chronic lymphocytic leukemia. *Blood*. 2017;129(11):1469-1479. doi:10.1182/blood-2016-06-719294
35. Komarova NL, Burger JA, Wodarz D. Evolution of ibrutinib resistance in chronic lymphocytic leukemia (CLL). *Proc Natl Acad Sci*. 2014;111(38):13906-13911. doi:10.1073/pnas.1409362111
36. Hillmen P, Rawstron AC, Brock K, et al. Ibrutinib plus Venetoclax in relapsed/refractory chronic lymphocytic leukemia: the CLARITY study. *J Clin Oncol*. 2019;37(30):2722-2729. doi:10.1200/JCO.19.00894
37. Lu P, Wang S, Franzen CA, et al. Ibrutinib and venetoclax target distinct subpopulations of CLL cells: implication for residual disease eradication. *Blood Cancer J*. 2021;11(2):1-14. doi:10.1038/s41408-021-00429-z

38. Lee DH, Hawk F, Seok K, et al. Association between ibrutinib treatment and hypertension. *Heart*. 2022;108(6):445-450. doi:10.1136/heartjnl-2021-319110
39. Uhm J. Recent advances in chronic lymphocytic leukemia therapy. *Blood Res*. 2020;55(Suppl):S72-S82. doi:10.5045/br.2020.S012
40. Rossi D, Rasi S, Spina V, et al. Integrated mutational and cytogenetic analysis identifies new prognostic subgroups in chronic lymphocytic leukemia. *Blood*. 2013;121(8):1403-1412. doi:10.1182/blood-2012-09-458265
41. O'Brien S, Furman RR, Coutre S, et al. Single-agent ibrutinib in treatment-naïve and relapsed/refractory chronic lymphocytic leukemia: a 5-year experience. *Blood*. 2018;131(17):1910-1919. doi:10.1182/blood-2017-10-810044
42. Wierda WG, O'Brien S, Wang X, et al. Prognostic nomogram and index for overall survival in previously untreated patients with chronic lymphocytic leukemia. *Blood*. 2007;109(11):4679-4685. doi:10.1182/blood-2005-12-051458
43. Sivina M, Xiao L, Kim E, et al. CXCL13 plasma levels function as a biomarker for disease activity in patients with chronic lymphocytic leukemia. *Leukemia*. 2021;35(6):1610-1620. doi:10.1038/s41375-020-01063-7
44. Gallais F, Ysebaert L, Despas F, et al. Population PK-PD modeling of circulating lymphocyte dynamics in chronic lymphocytic leukemia patients under Ibrutinib treatment. *Clin Pharmacol Ther*. 2021;110(1):220-228. doi:10.1002/cpt.2189
45. Herman SEM, Niemann CU, Farooqui M, et al. Ibrutinib-induced lymphocytosis in patients with chronic lymphocytic leukemia: correlative analyses from a phase II study. *Leukemia*. 2014;28(11):2188-2196. doi:10.1038/leu.2014.122
46. van Hasselt J, Gupta A, Hussein Z, Beijnen J, Schellens J, Huitema A. Integrated simulation framework for toxicity, dose intensity, disease progression, and cost effectiveness for castration-resistant prostate cancer treatment with Eribulin. *CPT Pharmacomet Syst Pharmacol*. 2015;4(7):374-385. doi:10.1002/psp4.48

SUPPORTING INFORMATION

Additional supporting information can be found online in the Supporting Information section at the end of this article.

How to cite this article: Ibrahim EIK, Karlsson MO, Friberg LE. Assessment of ibrutinib scheduling on leukocyte, lymph node size and blood pressure dynamics in chronic lymphocytic leukemia through pharmacokinetic-pharmacodynamic models. *CPT Pharmacometrics Syst Pharmacol*. 2023;12:1305-1318. doi:10.1002/psp4.13010